PCCP

Accepted Manuscript

ROYAL SOCIETY OF CHEMISTRY

www.rsc.org/pccp

Journal Name

RSCPublishing

ARTICLE

Investigation of PF_6^- and $TFSI^-$ anion intercalation into graphitized carbon blacks and its influence on high voltage lithium ion batteries

Cite this: DOI: 10.1039/xoxxoooooox

Received ooth January 2012,
Accepted ooth January 2012

DOI: 10.1039/xoxxoooooox

www.rsc.org/

Xin Qi [a], Berislav Blizanac [b], Aurelien DuPasquier [b], Paul Meister [a], Tobias Placke [a], Miodrag Oljaca [b], Jie Li [a,*] and Martin Winter [a,*]

Graphitized carbon blacks have shown a more promising electrochemical performance than the non-treated ones when being applied in small amounts as conductive additive in composite cathode electrodes for lithium ion batteries, due to the absence of surface functional groups which contribute to detrimental side-reactions with the electrolyte. Here, we report that at high potentials of >4.5 V *vs.* Li/Li^+, graphitic structures in carbon black can provide host sites for the partially reversible intercalation of electrolyte salt anions. This process is in analogy to the charge reaction of graphite positive electrodes in dual-ion cells. A standard furnace carbon black with small graphitic structural units, as well as slightly and highly graphitized carbon blacks, were characterized and analyzed with regard to anion intercalation. A $LiPF_6$ containing organic solvent based electrolyte as well as a state-of-the-art ionic liquid based electrolyte composed of LiTFSI in $PYR_{14}TFSI$, were applied. The intercalation of both PF_6^- and $TFSI^-$ could be confirmed by cyclic voltammetry in electrodes made from the carbon blacks. When exposed to high potentials, the carbon blacks experienced a strong activation in the 1st cycle, which promotes the perception for anion intercalation, and thus increases the anion intercalation capacity in the following cycles. The specific capacity from anion intercalation was evaluated by constant current charge/discharge cycling. The obtainable capacity was proportional to the graphitization degree. As anion intercalation might be accompanied by decomposition reactions of the electrolyte, e.g., by co-intercalation of solvent molecules, it could induce the decomposition of electrolyte inside the carbon and thus degradation of the carbon black graphitic structure. In order to avoid side reactions from surface groups and from anion intercalation, the thermal treatment of carbon blacks must be optimized.

1. Introduction

Currently, carbon black is the preferred choice as conductive carbon filler (CCF) in composite electrodes of lithium ion batteries because of its high contact surface area, low cost, and the long-term in-use experience by the cell manufacturers. Carbon black is a non-graphitic carbon[1-3], which contains groups of graphene-like layers, providing layer stacking with random orientation[4]. The carbon black primary particles are composed of a shell with concentric graphitic domains, and a more amorphous core. The relative ratio between graphitic and amorphous regions decreases gradually towards to the centre of carbon black particles. The average planar size of the crystalline graphite structures (L_a), their height (L_c), as well as the percentage of ordered (graphite-like) and disordered structures could be derived with the help of total X-ray scattering[5], atomic force microscopy[6] and Raman spectroscopy measurements[7, 8].

The graphite crystallite size in carbon blacks can be enlarged by heat-treatment. After being heated to >1,400 °C[1, 7, 9], the graphene layers are more conjointly oriented. The graphitization degree is increased as the heating temperature rises. However, the growth of the graphite crystallite domains by graphitization will be stopped by defects or when reaching the basal planes of a separate neighbouring graphite crystallite.

Therefore, carbon blacks can never be completely converted into graphite.

Both, cations, e.g. Li^+, and anions, e.g. PF_6^- [10], can be intercalated into graphite or carbon blacks[11]. From liquid organic electrolytes, this intercalation can take place as so-called solvated intercalation, meaning that the respective ions are intercalated together with the electrolyte solvent shell[10, 12-16]. When graphitized carbon blacks are applied as conductive additive in lithium ion batteries (LIBs), during charge the graphitic domains could provide intercalation sites for the electrolyte anions at the positive electrode (cathode). This phenomenon can be observed during charge at high cathode working potentials of >4.5 V *vs.* Li/Li^+, e.g. in 5.0 V LIBs[17-19].

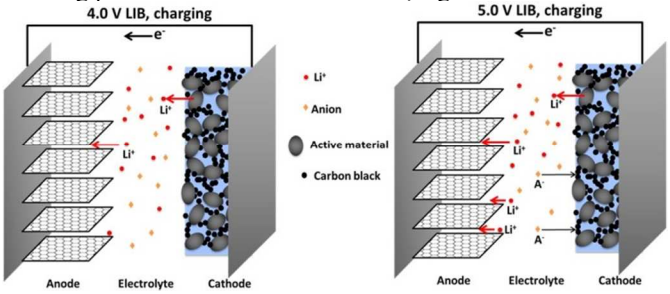

Figure 1: Schematic illustration of 4.0 and 5.0 lithium ion batteries during charge. The composite cathode is composed of binder, active material and carbon conductive filler additives (CCF); while the anode is e.g., composed of graphitic carbon (any carbon black additive and binder in the anode is disregarded for simplicity reasons). In an operation mode below 4.0 V (left), during charge, Li^+ is released from the cathode active material and intercalated into graphite. In a 5.0 V LIB (right), in parallel to Li^+-de-insertion from the cathode conductive salt anions in the electrolyte are intercalated into the CCF at the cathode. The corresponding amount of electrolyte salt Li^+-cations has to be intercalated into the anode for charge compensation in the electrolyte.

As shown in Figure 1, in the state-of-the-art LIBs operating below ca. 4.0 V, the Li^+ cations are released from the cathode active material into the electrolyte during charge; while simultaneously, Li^+ from the electrolyte will be intercalated into the anode material. The electrons move in parallel to the lithium ions to the anode via the external circuit. At contrast in "5.0" LIBs, when the cells are charged to >4.5 V *vs.* Li/Li^+, the cathode is highly polarized and the driving force is high enough to compel the conductive salt anions into the CCF at the composite cathode, especially when the CCF is graphitic. Li^+-de-insertion (from the cathode material) occurs in parallel to anion intercalation (into the CCF additive). This means, that in 5.0 V LIBs anion intercalation generates "extra" charge capacity at the cathode, which has to be balanced by an extra charge capacity at the anode. In other words, at the anode, the capacity is composed of Li^+ storage (stemming from the cathode material) and Li^+ storage (stemming from the electrolyte as counter-cation to the anion). The additional Li^+ from the electrolyte requires a higher anode material excess during cell assembly. This has an effect on the capacity balance in a lithium ion cell, because lithium ion cells work with an excess of anode material to avoid Li metal deposition on the anode surface during charge. The intercalated amount of anions depends on the size and the structure of the CCF particles. For those carbonaceous materials with highly graphitic structures, the amount of inserted anions could be notable and could even contribute to the total capacity[17-19].

In addition, the anion intercalation reaction may induce decomposition of electrolyte and degradation of the carbon black, thus degradation of the composite cathode, as discussed above. This suggests that a large amount of graphitic structural units in carbon black, which is created by heat-treatment at higher temperatures, should be avoided and this should be regarded in the carbon black manufacturing process.

Functional groups like hydroxyl-, carbonyl-, carboxyl- as well as quinone-, lactone-, aromatic- and phenolic groups do appear on the surface of carbon blacks[20-23]. In electrochemical reactions, the functional groups could act as highly reactive sites and are very likely to induce side reactions in lithium ion batteries, which can result in the decomposition of electrolyte components[24]. Those surface chemical groups can be partially removed by thermal treatment beyond the graphitization temperature[25, 26]. A "noble" carbon surface can be considered to be beneficial to the long-term cycling stability of the cell. Consequently, it is critical to evaluate the necessity of heat-treatment and to what degree the carbon blacks should be heat-treated and thus graphitized, to remove surface structures and functional groups while still avoiding the intercalation of anions.

In this work, three carbon blacks of different graphitization degrees were applied as cathode active material without any additional active cathode material. Organic solvent based electrolyte with the $LiPF_6$ electrolyte salt, as well as ionic liquid based electrolyte with the lithium bis(trifluoromethanesulfonyl) imide (LiTFSI) salt, were studied to verify the intercalation of different anions into carbon blacks. Electrochemical analysis included cyclic voltammetry (CV) and constant current charge/discharge cycling.

2. Experimental

Three carbon black samples (non-graphitized (CB1), slightly graphitized (CB2) and highly graphitized (CB3)) were applied in this work. Basic physical properties, including the N_2 BET specific surface area, average primary particle size and oil absorption number (OAN) of the samples are listed in Table 1. The planar crystallite domain diameter, L_a, as well as the crystallinity of each carbon black sample derived from Raman analysis is listed in Table 2.

Table 1: The BET surface area, primary particle size and oil absorption number (OAN) values of the carbon blacks used in this study.

Carbon black	CB1	CB2	CB3
N_2 BET surface area [$m^2\ g^{-1}$]	55	53	52
Average primary particle size [nm]	31	31	31
OAN [ml /100 g]	147	135	132

Table 2: The changes in the lateral crystalline domain size (L_a) and the crystallinity during the thermal graphitization process.

Carbon black	CB1	CB2	CB3
L_a [nm]	2.1	3.8	9.5
Crystallinity [%]	33	46	68

The structure of the carbon blacks before and after graphitization was characterized by X-ray diffraction (XRD, BRUKER D8 Advance X-ray diffractometer equipped with a copper target X-ray tube). X-ray photoelectron spectroscopy (XPS, Axis Ultra HSA, Kratos, GB) was used to investigate the difference in the surface chemistry of the non-graphitized and the graphitized carbon blacks, as well as the organic decomposition products after the cyclic voltammetry measurement. The source energy was supported by a monochromatic Al K_α source (h·v=1,486.6 eV), at a 10 mA filament current and a 12 kV filament voltage source energy. To compensate for the charging of the sample, a charge neutralizer was used. The pass energy was set as 20 eV. The analysis area was 700 µm × 300 µm. Calibration of the binding energy (BE) of the measured spectra was performed by using the energy of the C1s peak of carbon black (C-C, BE = 284.6 eV) as internal reference.

The electrodes contained 80 wt. % carbon black and 20 wt. % polyvinylidene difluoride (PVdF, Solef 5130, SOLVAY), as binder. N-methylpyrrolidone (NMP, ALDRICH) was used as dispersant. The binder was first made into a 6 wt. % solution in NMP, to guarantee a uniform cladding around carbon black particles. The slurry was homogenized by a planetary ball mill (Vario-Planetary Mill Pulverisette 4, FRITSCH) at 200 rpm for 4 hours to break possible carbon black agglomerates, and then cast onto aluminum foil. The electrodes were cut into 12 mm ø disk, and the mass loading of all the electrodes was controlled to be 0.9 mg cm^{-2} (including carbon black and binder) with a standard deviation of less than 0.03 mg cm^{-2}. Thus, the electrode rate performance can be expected to be free from mass loading deviation effects. All electrodes were dried under vacuum (< 0.01 mbar) at 120 °C for 12 h.

A solution of 1 M $LiPF_6$ in a 1:1 volume mixture of ethylene carbonate (EC) and dimethyl carbonate (DMC) from UBE was used as electrolyte. An ionic liquid based electrolyte, containing 0.3 M lithium bis(trifluoromethanesulfonyl) imide (LiTFSI, 3M) in 1-butyl-1-methylpyrrolidinium bis(trifluoromethanesulfonyl) imide ($PYR_{14}TFSI$, Solvionic) was used for comparison.

The cycling performance was tested in SwagelokTM cells (three-electrode set-up) with lithium metal (Rockwood Lithium, lithium battery grade) as counter and reference electrode. All the cells were assembled in a glove box with oxygen and water contents below 0.1 ppm and then equilibrated at 20 °C for 12 hours.

A VMP potentiostat (Biologic Science Instruments) was applied to carry out the cyclic voltammetry (CV) investigations. In the PF_6^- containing organic solvent-based electrolyte system, the CV was performed within the cut-off potentials of 2.5 - 5.2 V *vs.* Li/Li^+, with a scan rate of 20 mV s^{-1}; while, in the ionic liquid electrolyte based system, the cut-off potentials of 3.4 - 5.3 V *vs.* Li/Li^+. Taking into account the fact that the larger anion TFSI- might be more difficult to be intercalated, a lower scan rate of 0.1 mV s^{-1} was applied. Constant current cycling performance was measured by a Maccor™ series 4300 battery tester at 20 °C. The cycling performance was examined within different cut-off potential ranges with a specific current density of 100 mA g^{-1}. For each electrode system, at least two cells were tested to guarantee the reproducibility. All the potentials mentioned in this work refer to Li/Li^+.

3. Results and discussion

3.1 Characterization of carbon blacks

The XRD patterns of the three samples (CB1-3) (Figure 2) prove that the CBs have a different degree of graphitization. Even the low-graphitization sample CB1 showed three distinguishable signals (002), (100) and (110), which indicated a partially graphitic structure. For the more graphitized carbon blacks, these peaks were sharper and one additional reflection peak (004) appearing at 2θ = 54° (Figure 2), demonstrating a more ordered graphitic structure According to the ref.[27], completely graphitic structures can not be obtained by thermal treatment of carbon blacks.

In accordance with the trend shown in the XRD patterns (Figure 2): as the carbon black graphitization degree increases, the size of the graphitic domains as well as the total amount of crystallites increases, too (Table 2). Although carbon blacks will never reach the same crystallinity level as graphite, a large amount of graphitic structure can be generated after graphitization and therefore the carbon blacks show a certain graphite-like behaviour. According to our results, Li^+ intercalation into graphitized carbon blacks could be clearly confirmed and a discharge capacity of around 200 mAh g^{-1} can be obtained. This reaction with Li^+ would also affect other carbonaceous materials used at the anode, e.g. carbon coatings of the current collector or carbonaceous current collectors.

Also, as demonstrated in our previous work, large amounts of oxygen-containing groups are bound to the surface of carbon blacks, especially to the high energy sites, like edge sites at the prismatic surfaces. The surface of carbon blacks is therefore more susceptible to moisture adsorption. At high cathode potentials (≥4.7 V *vs.* Li/Li^+), these functional groups are highly active towards $LiPF_6$ when moisture exists in the electrolyte[28-30]. As shown in Figure 3, carbon-oxygen single bonds (alcohol or ether), carbon-oxygen double bonds (carbonyl, carboxyl or ester), carbonate or satellite species were found on the carbon black surface. After thermal treatment to achieve graphitic carbon blacks, a decrease of the oxygen containing groups was confirmed by a reduced relative ratio between the carbon-oxygen bonds (Peak 2, 3, 4) and the C-C bonds (Peak 1).

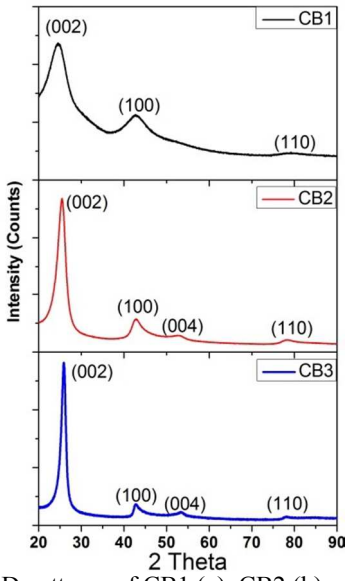

Fig. 2 (left): XRD patterns of CB1 (a), CB2 (b) and CB3 (c).

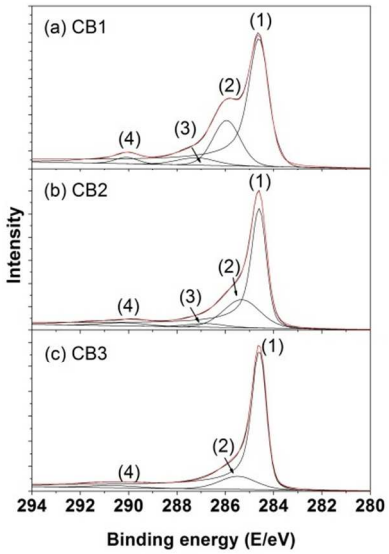

Fig. 3 (right): The C 1s spectrum of CB1 (a), CB2 (b) and CB3 (c).

Table 3: Peak components fitting of the C 1s spectrum.

		Binding energy (eV)		
Peak	Species	CB1	CB2	CB3
1	C-C (carbon black)	284.6	284.6	284.6
2	-C-OH, -C-O-C, -C=O	285.9	285.3	285.5
3	-COOH, -COOR	287.2	286.8	-
4	-CO3, Π-Π*	290.1	290.2	290.7

3.2 Intercalation of PF_6^- from organic solvent based electrolytes into carbon black

The three carbon black electrodes were first investigated in the organic carbonate solvent based electrolyte with 1 M $LiPF_6$ as electrolyte salt. Cyclic voltammetric analysis was used to determine whether PF_6^- can be intercalated into carbon blacks and at which potentials this intercalation takes place. The CB was exposed to a potential of 5.2 V *vs.* Li/Li^+ to cover the working potential of most cathode materials, e.g. the $LiNi_{0.5}Mn_{1.5}O_4$, which is usually oxidized to ca. 5.0 V *vs.* Li/Li^+. The three voltammetric experiments are shown in Figure 4.

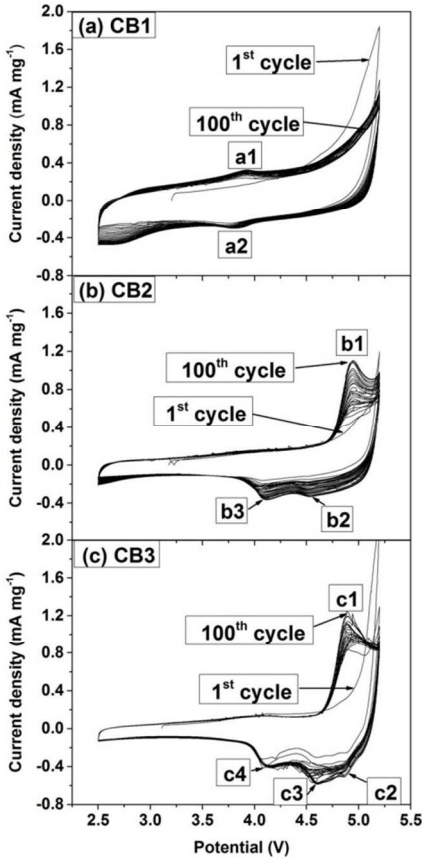

Figure 4: Cyclic voltammetric curves of (a) mostly amorphous carbon black (CB1), (b) slightly graphitized carbon black (CB2) and (c) highly graphitized carbon black (CB3) in 1 M $LiPF_6$ in EC: DMC (1:1) as electrolyte. Scan rate: 20 mV s^{-1}; cut-off potentials: 2.5 - 5.2 V *vs.* Li/Li^+.

A pair of redox peaks appeared in the voltammetric curve of the mostly amorphous CB1 (Figure 4a): the anodic peak at 3.92 V *vs.* Li/Li^+ (a1) and a corresponding cathodic peak at 3.75 V *vs.* Li/Li^+ (a2). These two peaks vanished in the voltammograms of the graphitized carbon blacks CB2 and CB3 (Figure 4b), where in addition to the observation of higher graphitization degree, also the amount of surface functional groups was reduced. This pair of peaks can be interpreted by a redox reaction between the organic solvent-based electrolyte and the carbon black surface functional groups.

With the slightly graphitized CB2, no obvious intercalation peak was observed in the first voltammetric cycle. However, from the second cycle on, an intercalation peak appeared at 4.94 V *vs.* Li/Li^+ (b1) and kept rising in the following cycles. Two corresponding cathodic peaks turned up at 4.54 V *vs.* Li/Li^+ (b2) and 4.11 V *vs.* Li/Li^+ (b3), and showed the same increasing behaviour during voltammetric cycling. The continuous current density increase of those peaks indicates a better accessibility of the intercalation sites of the carbon black. One may speculate that the better access to intercalation sites may facilitate the uptake of larger guest ions, e.g., the anion including a solvent shell. This can finally lead to an increase in

oxidative electrolyte decomposition reactions, which will influence the Coulombic efficiency.
Comparing CB2 with the even more graphitized CB3, the intercalation peak shifted to 4.89 V *vs.* Li/Li^+ (c1) and became sharper than for CB2. During the reduction sweep, three PF_6^- de-intercalation peaks at 4.86 V *vs.* Li/Li^+ (c2), 4.60 V *vs.* Li/Li^+ (c3) and 4.14 V *vs.* Li/Li^+ (c4), respectively, were observed. Still, the intensity of all the peaks showed an increasing trend during cycling.

For both CB2 and CB3, the intercalation took place around 4.9 V *vs.* Li/Li^+. In order to check the capacity from the PF_6^- intercalation reaction, constant current charge/ discharge cycling was performed within three cut-off potential windows: 3.5 - 4.4 V *vs.* Li/Li^+, 3.5 - 4.7 V *vs.* Li/Li^+, and 3.5 - 5.0 V *vs.* Li/Li^+ to evaluate the influence of the upper cut-off potential on the extent and reversibility of the PF_6^- intercalation reaction. All carbon blacks were cycled for 100 cycles in each cut-off potential window with a specific current of 100 mA g^{-1}. The specific charge/discharge capacities are shown in Figure 5.

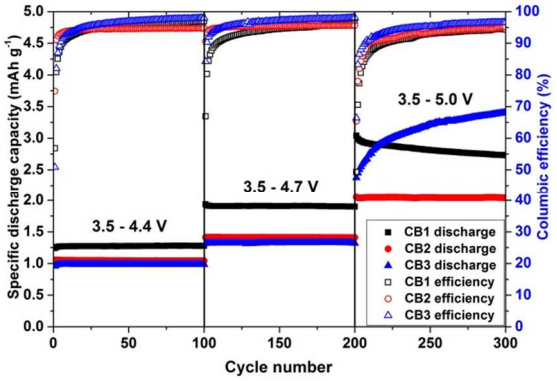

Figure 5: Specific discharge capacities and Coulombic efficiencies of CB1, CB2 and CB3 electrodes within different cut-off potential windows: 3.5 - 4.4 V *vs.* Li/Li^+ (the first 100 cycles); 3.5 - 4.7 V *vs.* Li/Li^+ (from cycle 101 to 200); 3.5 - 5.0 V *vs.* Li/Li^+ (from cycle 201 to 300). Specific current: 100 mA g^{-1}) in 1 M $LiPF_6$ in EC: DMC 1:1 (weight ratio) as electrolyte.

At a low upper cut-off potential of 4.4 V *vs.* Li/Li^+, where no PF_6^- intercalation can take place, but the redox reactions of the carbon black surface functional groups can contribute to the specific capacity, CB1 showed higher discharge capacities than the more graphitized carbon blacks. At the same time, the Coulombic efficiency of CB1 is lower than of the highly graphitized CB3. When the upper cut-off potential increased to 4.7 V *vs.* Li/Li^+, all three carbon blacks exhibited a capacity increase while the CB1 showed the highest capacity increase. Obviously, at higher potentials a larger contribution of the redox reaction of the surface groups to the overall discharge capacity could be observed. The strong capacity growth of CB1 at elevated potentials are a further proof for the peaks appearing in the voltammogram at 3.92 and 3.5 V *vs.* Li/Li^+ are caused by a different mechanism than the peaks observed in the voltammograms of CB2 and CB3. The capacity increase of CB1 can be explained by an enhanced extent of the surface group redox reactions at the higher potential of 4.7 V *vs.* Li/Li^+. As the surfaces of CB2 and CB3 were partially freed from surface groups after the thermal treatment, the capacities did not rise as much as that of CB1. When the cut-off potential was further increased to 5.0 V *vs.* Li/Li^+, the highly graphitized CB3 showed a dramatic intercalation capacity increase, and the capacity kept growing during cycling. Being slightly graphitized, CB2 possessed less surface functional groups than CB1; but CB2 is not as graphitic as CB3. Hence, the specific capacity of CB2 remained the lowest among the three. The capacity difference between CB2 and CB3 should be mainly caused by a larger extent of the PF_6^- intercalation reaction into CB3. In addition, the Coulombic efficiency of CB3 remained the highest among the three, which indicated that the insertion/de-insertion of PF_6^- into/from CB3 was highly reversible.

In the cyclic voltammograms (Figures 4b and c), CB2 and CB3 showed similarly shaped intercalation peaks, so they were expected to have a similar capacity when exposed to constant current cycling regime between 3.5 - 5.0 V *vs.* Li/Li^+. However, CB3 exposed a much higher capacity than CB2 in the constant current mode.

Back to the cyclic voltammetric curve of CB2, it must be noticed that during the first several cycles, the intercalation peak was not clearly visible, but the peak sharpened and increased in intensity as the cycling went on. To investigate, whether there is any influence of the upper cut-off potential on the specific capacity during cycling, CB2 was cycled by cyclic voltammetry within the cut-off potential range of 2.5 - 5.2 V *vs.* Li/Li^+ for 100 cycles. In parallel, the CB2 was cycled within the potential range of 3.5 - 5.0 V *vs.* Li/Li^+ (i.e. within the same potential window as for the constant current charge/ discharge experiment). Afterwards; the carbon blacks were charged and discharged with a constant current within the potential range of 3.5- 5.0 V *vs.* Li/Li^+ for 300 cycles.

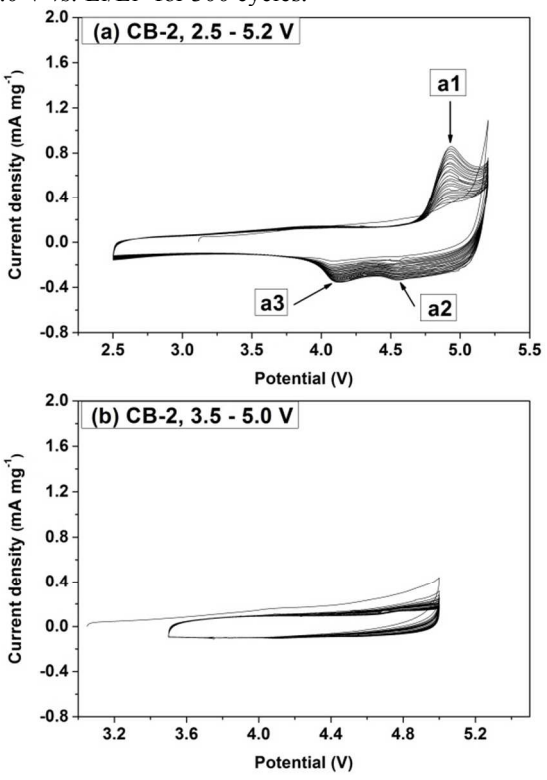

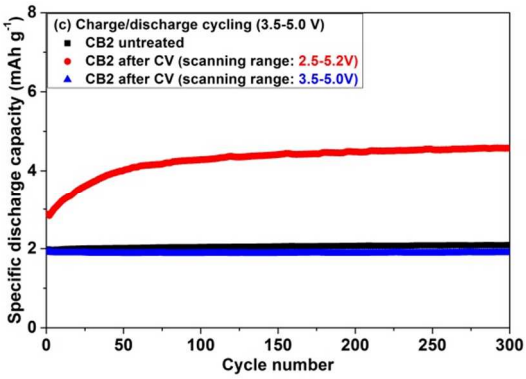

Figure 6: (a) Cyclic voltammetric curve of CB2 within the cut-off potential window (2.5 - 5.2 V *vs.* Li/Li^+) and (b) Cyclic voltammetric curve of CB2 within the cut-off potential window (3.5 - 5.0 V *vs.* Li/Li^+); the scan rate in both experiments was 20 mV s^{-1}; (c) constant current charge/discharge cycling of the untreated CB2 (black) and the treated CB2 samples. The CB2 sample which were first analysed in the cyclic voltammetric experiments between 2.5 - 5.2 V *vs.* Li/Li^+ is labelled as red, and the CB2 sample which was scanned within 3.5 - 5.0 V *vs.* Li/Li^+ is marked blue.

According to the cyclic voltammograms in Figures 6a and b, the intercalation peak showed a much lower intensity and no tendency in capacity increase when the CB2 was scanned between 3.5 to 5.0 V *vs.* Li/Li^+ than in the case when the CB2 is scanned between 2.5 and 5.2 V *vs.* Li/Li^+). This indicates that the intercalation of PF_6^- is limited at a lower cut-off potential of 5.0 V *vs.* Li/Li^+. After the cyclic voltammetric experiment at the low potential of 5.0 V *vs.* Li/Li^+ CB2 showed no difference in the constant current specific discharge capacity compared to the untreated CB2 (Figure 6c); while the CB2 electrode scanned to the higher potential of 5.2 V *vs.* Li/Li^+ possessed a constant current discharge capacity very similar to CB3 (see Figure 5), as well as the same trend in increasing capacity in the following cycles.

It can be concluded that the graphitic structure of the slightly graphitized CB2 is not as accessible to anions as the highly graphitized CB3. However, a high potential cut-off during the voltammetric scan could "activate" the structure to be more accessible to anion intercalation and thus could promote the reversible intercalation/de-intercalation of PF_6^-.

3.3 Intercalation of $TFSI^-$ from an ionic liquid based electrolyte into carbon black

Despite extraordinarily high costs, ionic liquids are considered to be one of the potential substitutes of organic solvent based electrolytes in the lithium ion batteries[31-33]. $TFSI^-$-anion based ionic liquids are less sensitive to side reactions with electrode components such as carbon surface groups than organic solvent based electrolytes containing $LiPF_6$. Therefore, it may be assumed that the application of ionic liquid as electrolyte can reduce the influence from redox reactions between the organic solvent based electrolyte and the carbon black surface groups. Simultaneously, the anodic stability can be extended up to 5.89 V *vs.* Li/Li^+ [34]. In this work, a state-of-the-art ionic liquid electrolyte, 0.3 M LiTFSI in $PYR_{14}TFSI$, was chosen to work with the carbon black electrodes. Intercalation of $TFSI^-$ into graphitic materials has been confirmed and been applied in the dual-ion cells[17-19, 35-37]. In these experiments it has also been confirmed that this electrolyte is compatible with the Al current collector without the Al dissolution problem happening in organic carbonate solvent based electrolytes[38, 39] However, no work so far has been focused on the intercalation of $TFSI^-$ into graphitized carbon blacks, to elucidate their reactivity as conductive additive in a LIB cathode.

The voltammetric measurements were performed within the cut-off potential range of 3.4 - 5.3 V *vs.* Li/Li^+ at a scan rate of 0.1 mV s^{-1} for 5 cycles. The slower scan rate was chosen because of the bigger ion size of $TFSI^-$ (3.9*8.0 Å) compared to PF_6^- (3.5*3.5 Å)[37], the intercalation process of $TFSI^-$ might be slower than that of PF_6^-. As shown in Figure 8a, in the CV curve of CB1 no redox peak similar to the one at 3.92 V *vs.* Li/Li^+ obtained in the organic solvent electrolyte (Figure 4a) was observed. In the voltammograms of CB2 and CB3 (Figures 7b and c), the intercalation peaks appeared, indicating that $TFSI^-$ was also inserted into the graphitized carbon blacks. The intercalation took place at 4.84 V *vs.* Li/Li^+ (b1) for CB2, and the de-intercalation peak arose at 4.41 V *vs.* Li/Li^+ (b2). For CB3, three intercalation peaks appeared at 4.64 V *vs.* Li/Li^+ (c1), 4.75 V *vs.* Li/Li^+ (c2) and 5.05 V *vs.* Li/Li^+ (c3), indicating that the highly graphitized carbon black possessed a structure which was more susceptible $TFSI^-$ intercalation. There appeared as many as four de-intercalation peaks which located at 5.03 *vs.* Li/Li^+ (c4), 4.90 *vs.* Li/Li^+ (c5), 4.73 *vs.* Li/Li^+ (c6) and 4.30 V *vs.* Li/Li^+ (c7). The understanding of the de-intercalation mechanism demands further investigations.

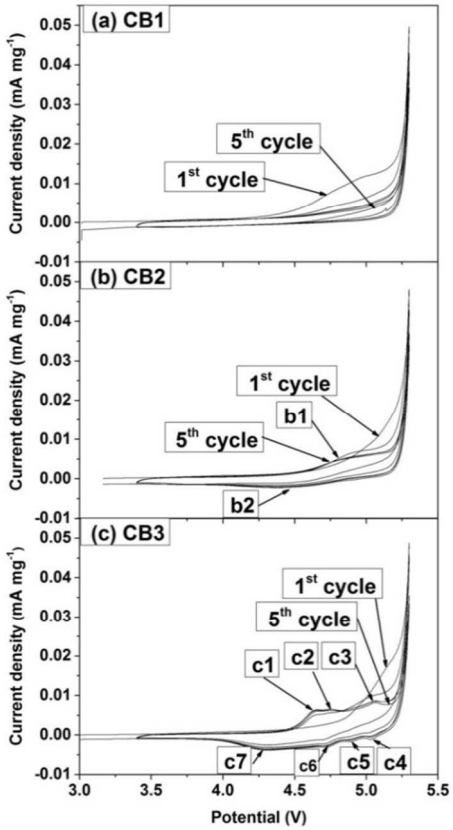

Figure 7: Cyclic voltammetric curves of (a) mostly amorphous carbon black (CB1), (b) slightly graphitized carbon black (CB2) and (c) highly graphitized carbon black (CB3) in 0.3 M LiTFSI in $PYR_{14}TFSI$ as electrolyte. Scan rate: 0.1 mV s^{-1}; cut-off potentials: 3.5 - 5.3V *vs.* Li/Li^+.

Based on the results of the voltammetric measurements revealing the potentials of the intercalation peaks, all electrodes were charged and discharged under constant current conditions for 30 cycles within two different cut-off potential windows: 3.5 - 4.4 V *vs.* Li/Li^+ and 3.5 - 5.2 V *vs.* Li/Li^+. The specific discharge capacities and Coulombic efficiencies are shown in Figure 8. Cycled below 4.4 V *vs.* Li/Li^+, all three carbon blacks delivered very similar discharge capacities. However, CB1 showed a slightly lower Coulombic efficiency than the other two carbon blacks, probably caused by irreversible surface group reactions. When the upper cut-off potential is extended to 5.2 V *vs.* Li/Li^+, the discharge capacities of all three carbon blacks increase; however, at the expense of lower Coulombic efficiencies. Under these cut-off potential conditions, the CB1 exhibited the lowest discharge capacity because the reactions of the surface groups are small in the ionic liquid based electrolyte, and the amorphous structure of CB1 was not suitable for a large extent of anion uptake. The low contribution of the surface groups of CB1 on the discharge capacity in the ionic liquid based electrolyte, gives rise to the speculation, that either the surface groups are not wetted in the ionic liquid based electrolyte, or that the reaction of the surface groups needs electrolyte components, which are only present in the organic solvent based electrolyte. As the graphitization degree increased, both the discharge capacities and the Coulombic efficiencies showed an increasing trend.

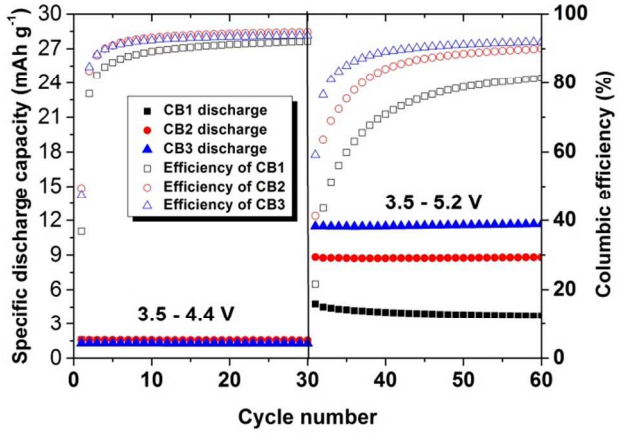

Figure 8: Specific discharge capacities and Coulombic efficiencies of CB1, CB2 and CB3 electrodes within two different cut-off potential windows: 3.5 - 4.4 V *vs.* Li/Li^+ (the first 30 cycles); 3.5 - 5.2 V *vs.* Li/Li^+ (cycle 31 to 60) at 1 C; 0.3 M LiTFSI in $PYR_{14}TFSI$ as electrolyte.

Conclusion

Carbon blacks have to be electrochemically stable at potentials >4.9 V *vs.* Li/Li^+ as conductive additive in high voltage composite LIB cathodes. In this work, it is confirmed that both PF_6^- and $TFSI^-$ anions can be reversibly intercalated into graphitized carbon blacks. The amount of intercalated anions highly depends on the graphitization degree. The continuous reversible intercalation and de-intercalation of the anions made the graphitic structure more susceptible to anion intercalation during long-term cycling in the case of graphitized carbon blacks. At contrast, no anion intercalation peaks were observed in the non-graphitized carbon black, but instead peaks due to the redox reactions of the surface groups.

This anion intercalation, in the case of organic solvent based electrolytes sometimes accompanied by the co-intercalation of solvent molecules, can expand the interlayer gaps between graphene layers, leading to increased irreversible reactions and the gradual structural degradation of carbon blacks. These reactions must be avoided when the graphitized carbon blacks are applied as conductive additives in high voltage cathodes (>4.9 V *vs.* Li/Li^+) in LIBs. However, thermal treatment of carbon blacks does not only lead to graphitization of the carbon, but also to the removal of detrimental surface groups which can cause irreversible reactions with the $LiPF_6$-containing organic solvent based electrolyte. Consequently, for the use of high voltage cathodes, the graphitization degree of carbon blacks must be optimized, aiming to remove surface functional groups but to not cause a high graphitization degree.

Acknowledgements

The authors thank the Cabot Corporation for the financial support and the supply of carbon black samples.

Notes and references

[a] MEET Battery Research Center, Institute of Physical Chemistry, University of Muenster, Corrensstraße 46, 48149 Muenster, Germany.
[b] Cabot Corporation, 5401 Venice Avenue NE, Albuquerque, NM 87113, USA.

1. R. E. Franklin, *Proc R Soc Lon Ser-A*, 1951, **209**, 196-&.
2. M. Liu, *Coating Technology of Nuclear Fuel Kernels: A Multiscale View*, 2013.
3. J. O. B. Martin Winter, *Handbook of Battery Materials*, 1999, **3**, 383-418.
4. J. Biscoe and B. E. Warren, *Journal of Applied Physics*, 1942, **13**, 364-371.
5. T. W. Zerda, W. Xu, A. Zerda, Y. Zhao and R. B. Von Dreele, *Carbon*, 2000, **38**, 355-361.
6. W. Xu, T. W. Zerda, H. Raab and D. Goritz, *Carbon*, 1997, **35**, 471-474.
7. T. Gruber, T. W. Zerda and M. Gerspacher, *Carbon*, 1994, **32**, 1377-1382.
8. T. W. Zerda, W. Xu, H. Yang and M. Gerspacher, *Rubber Chem Technol*, 1998, **71**, 26-37.
9. J. G. Zhao, L. X. Yang, F. Y. Li, R. C. Yu and C. Q. Jin, *Carbon*, 2009, **47**, 744-751.
10. T. Ishihara, Y. Yokoyama, F. Kozono and H. Hayashi, *J Power Sources*, 2011, **196**, 6956-6959.
11. J. Syzdek, M. Marcinek and R. Kostecki, *J Power Sources*, 2014, **245**, 739-744.
12. J. A. Seel and J. R. Dahn, *J Electrochem Soc*, 2000, **147**, 892-898.
13. H. Y. Wang and M. Yoshio, *Chem Commun*, 2010, **46**, 1544-1546.
14. M. R. Wagner, P. R. Raimann, A. Trifonova, K. C. Moller, J. O. Besenhard and M. Winter, *Anal Bioanal Chem*, 2004, **379**, 272-276.
15. H. J. Santner, C. Korepp, M. Winter, J. O. Besenhard and K. C. Moller, *Anal Bioanal Chem*, 2004, **379**, 266-271.

16. K. Tasaki, A. Goldberg and M. Winter, *Electrochim Acta*, 2011, **56**, 10424-10435.
17. T. Placke, P. Bieker, S. F. Lux, O. Fromm, H. W. Meyer, S. Passerini and M. Winter, *Z Phys Chem*, 2012, **226**, 391-407.
18. G. Schmuelling, T. Placke, R. Kloepsch, O. Fromm, H. W. Meyer, S. Passerini and M. Winter, *J Power Sources*, 2013, **239**, 563-571.
19. T. Placke, S. Rothermel, O. Fromm, P. Meister, S. F. Lux, J. Huesker, H. W. Meyer and M. Winter, *J Electrochem Soc*, 2013, **160**, A1979-A1991.
20. R. I. R. Blyth, H. Buqa, F. P. Netzer, M. G. Ramsey, J. O. Besenhard, P. Golob and M. Winter, *Appl Surf Sci*, 2000, **167**, 99-106.
21. R. I. R. Blyth, H. Buqa, F. P. Netzer, M. G. Ramsey, J. O. Besenhard and M. Winter, *J Power Sources*, 2001, **97-8**, 171-173.
22. M. L. Studebaker, E. W. D. Huffman, A. C. Wolfe and L. G. Nabors, *Ind Eng Chem*, 1956, **48**, 162-166.
23. J. S. Mattson and H. B. Mark, *J Colloid Interf Sci*, 1969, **31**, 131-&.
24. X. B. Li, Y. J. Chen, C. C. Nguyen, M. Y. Nie and B. L. Lucht, *J Electrochem Soc*, 2014, **161**, A576-A582.
25. T. Aida, N. Hirama and Y. Tsutsumi, *Abstr Pap Am Chem S*, 1997, **213**, 118-FUEL.
26. A. Bredin, A. V. Larcher and B. J. Mullins, *Tribol Int*, 2011, **44**, 1642-1650.
27. J. Lai, H. J. Guo, Z. X. Wang, X. H. Li, X. P. Zhang, F. X. Wu and P. Yue, *J Alloy Compd*, 2012, **530**, 30-35.
28. S. Y. Li, P. H. Ma, X. L. Cui, Q. D. Ren and F. Q. Li, *J Chem Sci*, 2008, **120**, 289-292.
29. J. S. Gnanaraj, E. Zinigrad, L. Asraf, H. E. Gottlieb, M. Sprecher, M. Schmidt, W. Geissler and D. Aurbach, *J Electrochem Soc*, 2003, **150**, A1533-A1537.
30. C. L. Campion, W. T. Li and B. L. Lucht, *J Electrochem Soc*, 2005, **152**, A2327-A2334.
31. A. Lewandowski and A. Swiderska-Mocek, *J Power Sources*, 2009, **194**, 601-609.
32. M. Galinski, A. Lewandowski and I. Stepniak, *Electrochim Acta*, 2006, **51**, 5567-5580.
33. S. F. Lux, M. Schmuck, G. B. Appetecchi, S. Passerini, M. Winter and A. Balducci, *J Power Sources*, 2009, **192**, 606-611.
34. M. Montanino, M. Moreno, F. Alessandrini, G. B. Appetecchi, S. Passerini, Q. Zhou and W. A. Henderson, *Electrochim Acta*, 2012, **60**, 163-169.
35. S. Rothermel, P. Meister, G. Schmuelling, O. Fromm, H.-W. Meyer, S. Nowak, M. Winter and T. Placke, *Energy & Environmental Science*, 2014, **7**, 3412-3423.
36. J. A. Read, A. V. Cresce, M. H. Ervin and K. Xu, *Energy & Environmental Science*, 2014, **7**, 3086-3086.
37. P. Meister, V. Siozios, J. Reiter, S. Klamor, S. Rothermel, O. Fromm, H.-W. Meyer, M. Winter and T. Placke, *Electrochim Acta*.
38. E. Kramer, T. Schedlbauer, B. Hoffmann, L. Terborg, S. Nowak, H. J. Gores, S. Passerini and M. Winter, *J Electrochem Soc*, 2013, **160**, A356-A360.
39. E. Kramer, S. Passerini and M. Winter, *Ecs Electrochem Lett*, 2012, **1**, C9-C11.